Xanthomonas type III effector XopN targets scaffold protein OsRACK1B to suppress rice immunity

Jiuxiang Wang[1,3,†], Zhe Ni[1,2,†], Xin Chen[1], Yaqi Zhang[1], Huajun Qin[1], Haoyu Wang[1], Yongqiang He[1,3], Jiliang Tang[1], Sheng Huang[1,*]

[1]State Key Laboratory for Conservation and Utilization of Subtropical Agro-bioresources, College of Life Science and Technology, Guangxi University, Nanning 530004, Guangxi, China

[2]College of Plant Protection, Northeast Agricultural University, Harbin 150030, Harbin, China

[3]College of Agriculture, Guangxi University, Nanning 530004, Guangxi, China

*Correspondence (Tel +8618076635685; email shuang@gxu.edu.cn)

[†]These authors have contributed equally to this work.

ABSTRACT

Bacterial leaf streak (BLS), caused by *Xanthomonas oryzae* pv. *oryzicola* (*Xoc*), is a major bacterial disease that poses a substantial threat to rice production. Although *Xoc* deploys a variety of effectors to subvert host defenses, the mechanistic basis of how these effectors modulate plant immune signaling remains largely unclear. Here, we show that XopN suppresses rice immune responses and physically interacts with the rice scaffold protein OsRACK1B. Notably, *OsRACK1B* expression is induced following *Xoc* infection in a type III secretion system (T3SS)-independent manner. Functional analyses indicate that *OsRACK1B* overexpression enhances *Xoc* resistance, whereas loss-of-function mutants exhibit heightened susceptibility. This increased susceptibility is characterized by compromised immunity, including reduced callose deposition, diminished reactive oxygen species (ROS) accumulation, and

attenuated expression of defense-related genes such as *OsPBZ1* and *OsPAL1*. Furthermore, we demonstrate that XopN competes with OsRap2.6 for binding to OsRACK1B, thereby disrupting the formation of the OsRACK1B–OsRap2.6 immune complex. These findings reveal a novel virulence strategy in *Xoc* and identify promising gene targets for developing disease-resistant rice varieties.

Keywords: *Xanthomonas oryzae* pv. *oryzicola*; rice; effectors; scaffold protein; immune responses

Introduction

Rice (*Oryza sativa* L.) is a staple crop that sustains the nutritional demands of more than half of the global population (Yuan et al., 2021). However, its productivity is continually threatened by a diverse array of pathogens and pests, which compromise both yield and grain quality (He et al., 2023). Among these, bacterial leaf streak (BLS), caused by *Xanthomonas oryzae* pv. *oryzicola* (*Xoc*), is a major bacterial disease that results in yield losses ranging from 8% to 32% (Liu et al., 2014). Genetically encoded resistance remains the most effective and environmentally sustainable approach for long-term disease management. Despite progress, only a limited number of resistance (*R*) genes, such as *Xo1*, *xa5*, *bls1*, and *OsBLS6.2*, have been identified as effective against BLS. (Ma et al., 2021; Triplett et al., 2016; Xie et al., 2023; Xie et al., 2014). This underscores the pressing need to elucidate the molecular strategies employed by *Xoc* to facilitate infection, which will be instrumental for the development of novel resistance traits.

The continuous co-evolution of pathogenic microbes and their host plants has led to the emergence of a sophisticated, two-layered innate immune system in plants: pattern-triggered immunity (PTI) and effector-triggered immunity (ETI) (Jones and Dangl, 2006; Wang et al., 2022). PTI is initiated upon recognition of conserved pathogen-associated molecular patterns (PAMPs) by pattern recognition receptors (PRRs) located at the plasma membrane (Li et al., 2016).

In contrast, ETI is activated intracellularly through nucleotide-binding leucine-rich repeat (NLR) receptors that detect pathogen-secreted effectors (Tsuda and Katagiri, 2010). Immune activation induces a range of defense responses, including the production of reactive oxygen species (ROS), callose deposition, mitogen-activated protein kinase (MAPK) cascade activation, upregulation of defense-related genes, and hypersensitive cell death (HR) at the site of infection (Gao et al., 2021; Spoel and Dong, 2012; Wang et al., 2020). While PTI provides basal immunity, ETI elicits a more robust and rapid defense, often accompanied by localized cell death to restrict pathogen spread (Spoel and Dong, 2012).

Many bacterial phytopathogens utilize a type III secretion system (T3SS) to translocate type III-secreted effectors (T3SEs) directly into host cells, where they manipulate host immunity and facilitate colonization (Boller and He, 2009). In *Xanthomonas* species, T3SEs are broadly classified into transcription activator-like (TAL) effectors and non-TAL effectors (Kay and Bonas, 2009). TAL effectors function as transcriptional activators upon nuclear import, often reprogramming host gene expression to support bacterial growth. For instance, TAL effectors from *X. oryzae* pv. *oryzae* (*Xoo*) induce *OsSWEET* gene expression, enabling pathogen exploitation of host sugars (Oliva et al., 2019). Similarly, the TAL effector Tal2g from *Xoc* promotes disease by upregulating the sulfate transporter gene *OsSULTR3;6* (Cernadas et al., 2014).

By contrast, non-TAL effectors exploit a diverse array of biochemical strategies to reprogram host cellular processes and facilitate bacterial colonization. For example, *X. campestris* pv. *vesicatoria* (*Xcv*) effector XopL functions as an E3 ubiquitin ligase that interacts with and degrades the autophagy component SH3P2, thereby promoting infection (Leong et al., 2022). Another effector, XopR from *X. campestris* pv. *campestris* (*Xcc*), forms biomolecular condensates via electrostatic-driven liquid–liquid phase separation (LLPS), coacervating with formin-mediated actin nucleation

complexes and manipulating the host cytoskeleton (Sun et al., 2021). Recent studies have increasingly highlighted the functional diversity of non-TAL effectors deployed by *Xoc*. For instance, XopC2 acts as a kinase that phosphorylates the Skp1 protein OSK1, thereby suppressing immune signaling (Wang et al., 2021). The effector AvrRxo1 degrades the pyridoxal phosphate synthase OsPDX1, reducing vitamin B6 levels and suppressing stomatal immunity (Liu et al., 2022). XopAP competitively binds phosphatidylinositol 3,5-bisphosphate (PtdIns(3,5)P2), inhibiting vacuolar acidification by interfering with vacuolar H^+-pyrophosphatase (V-PPase), ultimately promoting stomatal opening(Liu et al., 2022). More recently, XopAK was shown to repress *OsMYBxoc1* transcription and alter host iron homeostasis, thereby modulating rice immunity (Zhang et al., 2024).

Several non-TAL effectors, including AvrBs2, hrpE3 and XopN, have been identified as critical for the full virulence of *Xoc* (Cui et al., 2013; Li et al., 2015; Liao et al., 2020). However, the molecular mechanisms by which these effectors contribute to pathogenicity in rice remain largely unknown. Our previous study established that XopN significantly enhances the virulence of the *Xoc* strain GX01 (Liao et al., 2020). Here, we demonstrate that XopN suppresses rice immune responses and identify the rice scaffold protein OsRACK1B as a novel host target of XopN. Mechanistically, XopN impairs OsRACK1B function by disrupting its association with the transcription factor OsRap2.6, thereby dismantling a critical immune signaling complex. Functional analyses revealed that overexpression of *OsRACK1B* enhances rice resistance to *Xoc*, whereas *OsRACK1B* knockout lines exhibit heightened susceptibility and impaired immune responses. Collectively, these findings highlight a virulence strategy whereby XopN targets a central immune scaffold to suppress host defense, highlighting OsRACK1B as a promising molecular target for breeding BLS-resistant rice varieties.

112 ## Results

113 ### Δ*xopN* mutant elicits elevated rice immune responses

114 To gain insights into the evolutionary conservation of XopN, we performed a
115 BLAST analysis using its amino acid sequence as a query. The results revealed
116 that XopN is highly conserved within the *Xanthomonas* genus, exhibiting 96.0%
117 sequence identity with its homolog in *Xoo*, 81.7% identity with the counterpart
118 in *Xcc*, and 60.9% identity with the homolog in *Xcv* (Figure S1). Notably, a
119 putative homolog sharing 52.5% identity was also identified in *Acidovorax citrulli*,
120 a vascular pathogen of cucurbits, suggesting potential horizontal conservation
121 beyond the *Xanthomonas* clade. In contrast, XopN shows limited sequence
122 similarity to effector-like proteins from more distantly related phytopathogens,
123 such as *Ralstonia solanacearum* (25.2% identity), indicating that XopN and its
124 functional equivalents are largely restricted to *Xanthomonas* and a few
125 phylogenetically proximate taxa.

126 We further investigated the functional role of the *Xoc* effector XopN in
127 modulating rice innate immunity by comparing host responses triggered by the
128 wild-type strain GX01, the Δ*xopN* mutant, and the complemented strain
129 CΔ*xopN*. Callose, a β-1,3-glucan polymer, serves as a critical component of
130 plant immune defenses by reinforcing cell walls to restrict pathogen ingress and
131 dissemination (Li et al., 2023). Accordingly, we first assessed callose deposition
132 in rice leaves infiltrated with GX01, Δ*xopN*, or CΔ*xopN*. The results revealed
133 that leaves infected with the Δ*xopN* mutant exhibited significantly enhanced
134 callose accumulation relative to those inoculated with either GX01 or CΔ*xopN*
135 (Figure 1a,b). We next assessed ROS production, a rapid defense response
136 typically associated with PTI activation. Using 3,3′-diaminobenzidine (DAB)
137 staining, we observed a marked increase in H_2O_2 accumulation in Δ*xopN*-
138 infected leaves compared to those infected with GX01 or CΔ*xopN* (Figure 1c).
139 To determine whether XopN also modulates transcriptional defense responses,

140 we conducted quantitative reverse transcription PCR (RT–qPCR) to analyze
141 the transcript levels of canonical defense marker genes. The expression of
142 *OsPBZ1* and *OsPAL1* was significantly upregulated in Δ*xopN*-infected leaves
143 compared to GX01 (Figure 1d,e), indicating that XopN suppresses
144 transcriptional activation of these defense-associated genes.

145 Effectors are translocated into host cells to target various subcellular
146 compartments, manipulating diverse physiological and immune processes (Lo
147 Presti et al., 2015). To determine the subcellular localization of XopN, we
148 expressed XopN-GFP in rice protoplasts. The fusion protein was primarily
149 localized to the plasma membrane (PM) and cytoplasm (Figure 1f). Together,
150 these results demonstrate that XopN functions to dampen rice immune
151 responses at multiple levels, including callose deposition, ROS production, and
152 defense gene induction.

153 **XopN targets the scaffold protein OsRACK1B in rice**

154 To identify potential rice targets of XopN, we conducted a yeast two-hybrid (Y2H)
155 screen using a rice cDNA library with XopN as bait. This screen identified
156 OsRACK1B, a scaffold protein, as a putative interactor of XopN. To confirm this
157 preliminary interaction, full-length coding sequences of XopN and OsRACK1B
158 were cloned into the pGBKT7 (bait) and pGADT7 (prey) vectors, respectively.
159 Y2H assays confirmed that XopN interacts with OsRACK1B in yeast (Figure
160 2a). To further substantiate this interaction, we performed a reciprocal Y2H
161 assay in which full-length OsRACK1B was cloned into the pGBKT7 vector and
162 XopN into pGADT7. This reversed configuration also yielded a positive
163 interaction signal (Figure 2a). To assess whether this interaction occurs in
164 planta, we performed a bimolecular fluorescence complementation (BiFC)
165 assay in rice protoplasts. Yellow fluorescence was observed only upon co-
166 expression of nYFP–XopN and RACK1B–cYFP (Figure 2b), indicating a
167 specific interaction between the two proteins. Additionally, a pull-down assay

168 was conducted to validate the interaction in vitro. His-tagged XopN was
169 specifically pulled down by GST–RACK1B, but not by GST alone, further
170 supporting the direct interaction (Figure 2c).

171 We next mapped the interaction domains between XopN and OsRACK1B
172 using the Y2H system. A series of XopN truncations fused to GAL4-AD were
173 co-expressed with BD-OsRACK1B in yeast. The results indicated that the C-
174 terminal region of XopN (amino acids 240–358) is necessary for the interaction
175 (Figure 2d). Similarly, truncated OsRACK1B constructs were tested for their
176 ability to bind XopN, revealing that the WD7 domain alone was sufficient to
177 mediate the interaction (Figure 2e). Together, these data demonstrate that
178 XopN physically interacts with OsRACK1B both in vivo and in vitro and that this
179 interaction is mediated by specific regions within each protein.

180 ***OsRACK1B* gene expression is upregulated upon *Xoc* infection**

181 OsRACK1B encodes a 336-amino-acid protein containing seven WD40 repeats,
182 a domain architecture highly conserved across eukaryotic organisms (Figure
183 S2a). Phylogenetic analysis revealed that OsRACK1B shares the highest
184 sequence identity with its paralog OsRACK1A in rice (83.8%) and displays
185 greater similarity to orthologs in monocot species, including maize ZmRACK1
186 (82.5%) and wheat TaRACK1A (80.5%), than to those in dicots such as tobacco
187 NtRACK1 (68.8%) and *Arabidopsis* AtRACK1C (68.4%) (Supplementary Figure
188 S4B). Moderate sequence conservation was also observed with human (61.7%)
189 and yeast (44.0%) RACK1 homologs (Figure S2b), underscoring a deep
190 evolutionary relationship within the eukaryotic lineage. Notably, no RACK1
191 homologs have been identified in bacterial genomes, suggesting that RACK1
192 family proteins are unique to eukaryotes.

193 To determine whether *Xoc* infection alters *OsRACK1B* transcript levels, we
194 analyzed *OsRACK1B* mRNA abundance in rice leaves following inoculation
195 with the wild-type *Xoc* strain GX01. RT–qPCR revealed that *OsRACK1B*

196 expression was significantly induced at 12 and 24 hours post-inoculation (hpi)
197 (Figure 3a), indicating transcriptional upregulation in response to pathogen
198 challenge. To examine whether this induction depends on the T3SS, we
199 examined *OsRACK1B* mRNA levels in rice leaves inoculated with a T3SS-
200 deficient mutant (Δ*hrcC*). The expression of *OsRACK1B* was induced to a
201 similar level compared to the leaves infected with GX01 (Figure 3b), suggesting
202 that the induction of *OsRACK1B* is independent of the bacterial T3SS.

203 **OsRACK1B plays a positive role in rice resistance against *Xoc***

204 To determine the subcellular localization of OsRACK1B, we co-expressed
205 OsRACK1B-CFP with the nuclear marker ABF1-mCherry in rice protoplasts.
206 The CFP signal was observed in the plasma membrane, cytoplasm, and
207 nucleus (Figure 3c), indicating that OsRACK1B is a multi-compartmental
208 protein. To further investigate the functional role of *OsRACK1B* in rice
209 responses to *Xoc*, we generated stable transgenic rice lines constitutively
210 overexpressing *OsRACK1B* under the control of the CaMV 35S promoter via
211 *Agrobacterium tumefaciens*-mediated transformation. A total of fifteen
212 independent T_0 transgenic lines were confirmed by PCR and subsequently
213 advanced to the T_2 generation. Among these, two independent homozygous
214 overexpression lines, designated RACK1BOE-2 and RACK1BOE-3, exhibited
215 elevated OsRACK1B transcript abundance compared to wild-type NIP plants
216 and were selected for subsequent functional analyses (Figure 3d). To evaluate
217 the impact of *OsRACK1B* overexpression on BLS resistance, we inoculated
218 transgenic and wild-type plants with *Xoc* strain GX01. At 14 days post-
219 inoculation (dpi), both RACK1BOE lines displayed significantly reduced lesion
220 lengths compared to wild-type controls, indicative of enhanced resistance to
221 *Xoc* infection (Figure 3e,f).

222 We also generated *OsRACK1B* knockout mutants using CRISPR–Cas9-
223 mediated genome editing. Two independent knockout lines, OsRACK1BKO-2

224 and OsRACK1BKO-8, were identified. PCR amplification and sequencing
225 analysis revealed that OsRACK1BKO-2 carried a 2-bp deletion and a 1-bp
226 insertion at the U6a-gRNA and U6b-gRNA target sites, respectively, whereas
227 OsRACK1BKO-8 harbored a 1-bp insertion at both target sites (Figure 4a).
228 Following GX01 inoculation, lesion lengths in the knockout plants were
229 significantly greater than those in wild-type controls (Figure 4b,c). Together,
230 these findings indicate that *OsRACK1B* functions as a positive regulator of
231 resistance to BLS in rice.

232 **Knockout of *OsRACK1B* suppresses the rice immune response**

233 To gain mechanistic insights into the role of OsRACK1B in rice innate immunity,
234 we assessed callose deposition in *OsRACK1B* knockout mutants. Following
235 inoculation with the Δ*hrcC* mutant strain, the knockout lines exhibited a marked
236 reduction in callose accumulation in leaf tissues compared to wild-type plants
237 (Figure 5a,b). In parallel, DAB staining indicated that Δ*hrcC*-induced ROS
238 production was substantially attenuated in the knockout mutants relative to the
239 wild type (Figure 5c). To further explore the impact of *OsRACK1B* on immune
240 signaling, we quantified the transcript levels of two defense-related genes,
241 *OsPBZ1* and *OsPAL1*, in the mutant lines. RT–qPCR analysis revealed a
242 significant downregulation of both genes following Δ*hrcC* challenge in
243 OsRACK1B knockout plants compared to wild-type controls (Figure 5d,e).
244 These observations suggest that OsRACK1B contributes to PTI by regulating
245 callose deposition, ROS accumulation, and defense gene expression.

246 **XopN impairs the OsRACK1B–OsRap2.6 interaction**

247 The transcription factor OsRap2.6 plays a pivotal role in rice innate immunity
248 through its interaction with RACK1 (Wamaitha et al., 2012; Yoshihisa et al.,
249 2022). In the present study, we first confirmed the physical association between
250 OsRap2.6 and OsRACK1B using Y2H assays (Figure S3). Given that the
251 bacterial effector XopN also binds to OsRACK1B, we hypothesized that XopN

252 might modulate the OsRACK1B–OsRap2.6 interaction. Therefore, we first
253 employed AlphaFold3 prediction to investigate this hypothesis. The results
254 showed that the predicted interaction score between OsRACK1B and
255 OsRap2.6 was 0.65, which decreased substantially to 0.25 upon the addition
256 of XopN, suggesting that XopN may inhibit the interaction between OsRACK1B
257 and OsRap2.6 (Figure 6a). To validate this finding, we employed yeast three-
258 hybrid (Y3H) assays to assess the OsRACK1B–OsRap2.6 interaction in the
259 presence of either full-length. XopN or a truncated variant, XopN1–358. Notably,
260 co-expression of either form of XopN significantly attenuated the interaction
261 between OsRACK1B and OsRap2.6 (Figure 6b). These findings suggest that
262 XopN competitively disrupts the association between OsRACK1B and
263 OsRap2.6, potentially interfering with downstream immune signaling.

264 Discussion

265 T3SEs are key virulence determinants in Gram-negative bacterial pathogens
266 that actively manipulate host cellular processes to promote infection(Kay and
267 Bonas, 2009). These effectors are known to specifically target host substrates,
268 thereby suppressing immunity and enhancing pathogen proliferation. In the
269 present study, we demonstrate that *Xoc* effector XopN facilitates bacterial
270 infection by targeting the rice scaffold protein OsRACK1B, a positive regulator
271 of innate immunity. During infection, XopN is translocated into host cells via the
272 T3SS and competes with OsRap2.6 for binding to OsRACK1B. This competitive
273 interaction leads to impaired immune signaling, as evidenced by reduced
274 callose deposition, attenuated ROS accumulation, and downregulation of
275 defense-related gene expression, thereby promoting successful colonization of
276 host tissues by *Xoc* (Figure 6c).

277 To establish a successful infection, many host-adapted bacterial pathogens
278 deploy T3SEs that suppress plant immune responses from within host cells.
279 Previous research has demonstrated that *Xcv* effector XopN inhibits callose

280 deposition in both tomato and *Arabidopsis thaliana* (Kim et al., 2009). In line
281 with these findings, we observed that XopN from *Xoc* also suppresses callose
282 accumulation in rice (Figure 1a,b), suggesting a conserved effector function
283 across diverse plant species. Moreover, XopN inhibited ROS generation and
284 downregulated the expression of defense-related genes (Figure 1c-e).
285 Collectively, these data indicate that XopN enhances *Xoc* virulence by broadly
286 attenuating multiple layers of basal immune defense.

287 Phytopathogen effectors have evolved to subvert host immunity through
288 direct interactions with plant proteins, thereby undermining defense signaling
289 pathways (Dodds and Rathjen, 2010). In the present work, we provide multiple
290 lines of evidence by Y2H, in vitro pull-down and BIFC assays showing that
291 XopN interacts with the rice scaffold protein OsRACK1B (Figure 2). Previous
292 studies have shown that *Xcv* XopN is localized to both the PM and the
293 cytoplasm (Kim et al., 2009). Our analysis of XopN localization in planta, using
294 transient expression of XopN-GFP in rice protoplasts, supports this finding
295 (Figure 1f). OsRACK1B is localized in the PM, cytoplasm, and nucleus
296 (Supplementary Figure 3c), suggesting that the localization of OsRACK1B
297 partially overlaps with that of XopN in plant cells. However, whether the
298 interaction between XopN and OsRACK1B in these subcellular compartments
299 is essential for full resistance remains unclear. Future studies will be necessary
300 to delineate the precise subcellular locations of their interaction and further
301 explore the molecular functions of XopN in plant immunity.

302 In *Arabidopsis*, the three RACK1 homologs AtRACK1A, AtRACK1B, and
303 AtRACK1C have been implicated in a wide range of physiological processes,
304 including developmental regulation, hormone signaling, innate immunity, and
305 responses to abiotic stress (Chen et al., 2006; Cheng et al., 2015; Islas-Flores
306 et al., 2015). Rice encodes two homologs, OsRACK1A and OsRACK1B. While
307 overexpression of OsRACK1A has been reported to promote ROS
308 accumulation and enhance resistance to *Ustilaginoidea virens* and

309 *Magnaporthe oryzae* (Li et al., 2022; Nakashima et al., 2008), the functional
310 role of OsRACK1B in immunity has remained largely unexplored. Here, we
311 show that OsRACK1B expression is transcriptionally upregulated during the
312 early stages of infection, as revealed by RT-qPCR analysis (Figure 3a-b),
313 suggesting a role in basal defense against *Xoc*. This hypothesis was further
314 substantiated by resistance assays in OsRACK1B-overexpression and
315 knockout lines (Figure 3 c-e and Figure 4). Further functional analysis revealed
316 that OsRACK1B is essential for Δ*hrcC*-triggered callose deposition, ROS
317 production, and transcriptional activation of defense-related genes in rice
318 (Figure 5). Collectively, these findings identify OsRACK1B as a positive
319 regulator of rice immunity and suggest that it may serve as a critical node in the
320 defense signaling network against *Xoc* infection.

321 Scaffold protein RACK1 serves as a pivotal integrative hub in eukaryotes,
322 coordinating diverse signaling pathways through interactions with numerous
323 protein partners (Fu et al., 2024; Islas-Flores et al., 2015). Prior studies have
324 demonstrated that RACK1 forms a complex with the transcription factor Rap2.6,
325 a module implicated in rice immunity against *M. oryzae* (Guo and Sun, 2017;
326 Wamaitha et al., 2012). More recently, OsRap2.6 has been shown to regulate
327 NLR Xa1-mediated immunity in response to TAL effector recognition,
328 underscoring its central role in pathogen resistance signaling (Yoshihisa et al.,
329 2022). Here, we report that the *Xoc* effector XopN disrupts the interaction
330 between OsRACK1B and OsRap2.6 (Figure 6a,b). However, the functional
331 consequence of this disruption on OsRap2.6 remains unclear. Based on
332 structural and functional considerations, we speculate that XopN may affect the
333 stability or transcriptional activity of OsRap2.6. This mechanism is reminiscent
334 of the interaction between *Xcv* effector XopN and the tomato proteins TFT1 and
335 TARK1, where XopN promotes the formation of TFT1-TARK1 complex (Kim et
336 al., 2009; Taylor et al., 2012). Notably, in contrast to the stabilizing effect
337 observed in tomato, XopN in rice appears to dismantle the OsRACK1B–

338 OsRap2.6 complex, suggesting a species-specific modulation by this
339 evolutionarily conserved effector. Structural elucidation of XopN would likely
340 reveal the molecular basis of its interaction with the OsRACK1B–OsRap2.6
341 subcomplex and offer mechanistic insights into its mode of action.

342 In conclusion, our findings reveal a potential pathogenic mechanism through
343 which *Xoc* type III effector XopN targets the rice scaffold protein OsRACK1B to
344 attenuate basal immunity and promote bacterial colonization. This work
345 deepens current understanding of non-TALE-mediated host–pathogen
346 interactions and holds implications for the development of disease-resistant rice
347 cultivars.

348 **Materials and Methods**

349 **Plants and bacterial strains**

350 Rice cultivar Nipponbare was used as the wild-type (WT) control in this study.
351 For the overexpression of OsRACK1B, its coding sequence was PCR-amplified
352 and cloned into the pCAMBIA1301-HA binary vector. To generate knockout
353 lines, two guide RNAs targeting the coding region of OsRACK1B were designed
354 using the CRISPR-GE online toolkit (Xie et al., 2017). The gRNA expression
355 cassettes were subsequently inserted into the pYLCRISPR/Cas9 binary vector.
356 Both overexpression and CRISPR constructs were introduced into *Nipponbare*
357 via *A. tumefaciens*-mediated transformation (Wuhan BioRun Biosciences Co.,
358 Ltd.). Rice plants were cultivated in greenhouse conditions under a 14-hour light
359 (30°C)/10-hour dark (28°C) photoperiod.

360 *E. coli* and *A. tumefaciens* strains were propagated in LB medium at 37°C
361 and 28°C, respectively. *Xoc* strains were cultured at 28°C in NB medium
362 (polypeptone 5g/L, beef paste 3g/L, yeast extract 1g/L, sucrose 10g/L).
363 Virulence assays were conducted as previously described (Wang et al., 2024).
364 Briefly, *Xoc* strains were resuspended in sterile distilled water to an optical

365 density of OD_{600} = 0.5 and infiltrated into rice leaves using needleless syringes.
366 Lesion lengths were recorded, and photographs were taken 14 days post-
367 inoculation.

368 **RNA analysis**

369 Total RNA was extracted from rice leaf tissue using TRIzol Reagent (Invitrogen,
370 Cat# 15596018, USA) according to the manufacturer's protocol. First-strand
371 cDNA synthesis was performed with the RevertAid First Strand cDNA Synthesis
372 Kit (Thermo Fisher Scientific, Cat# K1622, USA). Quantitative real-time PCR
373 (RT-qPCR) was conducted using the qTOWER 2.2 Real-Time PCR Detection
374 System (Analytik Jena, Germany) with ChamQ SYBR Color qPCR Master Mix
375 (Vazyme, Cat# Q411-02, China), following the manufacturer's instructions.
376 OsACTIN1 was used as the internal reference gene to normalize transcript
377 levels. Relative gene expression was calculated using the $2^{-\Delta\Delta CT}$ method.
378 Primer sequences used in this study are listed in Table S1.

379 **Callose deposition and DAB staining**

380 Leaves from 2–3-week-old rice seedlings inoculated with *Xoc* were fixed in
381 ethanol: acetic acid (3:1, v/v) for 5 h, with frequent replacement of the solution
382 until fully decolorized. Samples were subsequently rehydrated through a
383 graded ethanol series (70% for 2 h, 50% for 2 h), followed by incubation in
384 distilled water overnight. After triple rinsing with water, the tissues were cleared
385 by incubation in 10% (w/v) NaOH for 1 h. Leaves were then washed four times
386 with water and stained in 0.01% aniline blue solution (150 mM K_2HPO_4, pH 9.5)
387 for 4 h. Callose deposits were visualized immediately using a fluorescence
388 microscope equipped with a UV filter(Deb et al., 2020).

389 For DAB staining, inoculated rice leaves were collected and incubated in DAB
390 solution (1 mg/mL, Sigma Aldrich) for 24 h with gentle agitation. Leaves were
391 subsequently cleared in a decolorizing solution composed of ethanol, acetic

392 acid, and glycerol (3:1:1, v/v/v) before imaging(Deb et al., 2020).

393 **Y2H assay and Y3H assay**

394 The Matchmaker gold Y2H system (Clontech) was used to screen XopN-
395 interacting proteins. The XopN coding sequence was cloned into the bait vector
396 pGBKT7 and then transformed into the yeast strain Y2H gold. A rice cDNA
397 library was constructed into the prey vector pGADT7 using mRNA extracted
398 from rice leaves according to the manufacturer's protocol. Positive interactors
399 were initially selected on SD/-Leu/-Trp/-His/-Ade dropout medium. To validate
400 the interaction between XopN and OsRACK1B, their coding sequences were
401 individually cloned into pGBKT7 and pGADT7, respectively, and co-
402 transformed into the Y2HGold strain. Transformed yeast colonies were selected
403 on SD/-Leu/-Trp plates, and interactions were assessed by growth on
404 quadruple dropout medium (SD/-Leu/-Trp/-His/-Ade).

405 For the Y3H assay, the pBridge vector was used to express both XopN and
406 OsRACK1B. The pGADT7 vector was used to express OsRap2.6. The
407 recombinant constructs were co-transformed into the yeast strain Y2HGold.
408 Transformants were selected on SD/-Met/-Trp/-Leu medium, and protein–
409 protein interactions were assessed by growth on SD/-Met/-Trp/-Leu/-His/-Ade
410 selective plates.

411 **Pull-down assay**

412 The XopN coding sequence was cloned into the vector pET28a to generate His-
413 XopN fusion protein. The coding sequence of OsRACK1B was cloned into the
414 vector pGEX-6p-1 to generate GST-OsRACK1B fusion protein. His-XopN and
415 GST-OsRACK1B were expressed in *E. coli* strain BL21 and were purified with
416 Ni-NTA resin and GST resin, respectively (Transgen). His-XopN proteins were
417 immobilized on Ni-NTA resin and incubated with GST-OsRACK1B or GST at
418 4°C for 4 h with gentle shaking. After five times washing with 1 × PBS (4.2 mM

419 Na_2HPO_4, 2 mM KH_2PO_4, 140 mM NaCl, and 10 mM KCl), the mixtures were
420 eluted using the elution buffer. Last, the elution samples were boiled with 5 ×
421 SDS loading buffer at 100°C for 5 min for immunoblot analysis.

422 **BIFC assay**

423 The pXY104 and pXY106 plasmids were used for the BIFC assay(Fu et al.,
424 2025). The coding sequence of XopN was cloned into pXY106 to make the
425 XopN-nYFP fusion protein. The OsRACK1B coding sequence was cloned into
426 pXY104 to make the OsRACK1B-cYFP fusion protein. The constructs were co-
427 expressed in rice protoplasts. The YFP fluorescence was observed using a
428 confocal laser scanning microscope (Leica TCS SP8 MP).

429 **Subcellular localization**

430 To examine the subcellular location of XopN and OsRACK1B, full-length cDNAs
431 were constructed into vector pBWA(V)HS-GFP and pBWA(V)HS-GFP to make
432 the fusion proteins XopN-GFP and OsRACK1B-CF, respectively. The
433 recombinant plasmids were transfected into rice protoplasts, and the
434 fluorescence was observed using a confocal laser scanning microscope at 24
435 h after transfection.

436 **Sequence alignment and phylogenetic analysis**

437 Orthologs of XopN from various bacterial species were identified and retrieved
438 from the NCBI database. Protein sequences were aligned using the Constraint-
439 based Multiple Alignment Tool (COBALT), and the resulting alignments were
440 visualized with the online software ESPript 3.0 (Robert and Gouet, 2014). NCBI
441 BLASTP was used to select and download the orthologs of OsRACK1B in other
442 plants. A phylogenetic tree was constructed with MEGA 7.0 using the maximum
443 likelihood (ML) method and 1,000 bootstrap replicates.

444 **Accession numbers**

445 The sequence data from this article can be found on the Kyoto Encyclopedia of
446 Genes and Genomes website (https://www.kegg.jp/) under the following
447 numbers: *xopN* (*Xoc_0350*), *OsRACK1B* (*Os05g0552300*), *OsPBZ1*
448 (*Os12g0555500*), *OsPAL1* (*Os02g0626100*), *OsRap2.6* (*Os04g0398000*) and
449 *OsACTIN* (*Os03g0718100*).

450 **Author contributions**

451 S.H. conceived the research and designed the experiments. J.W., Z.N., X.C.,
452 Y.Z. and H.Q. performed the experiments; J.W., Z.N. and H.W. analysed the
453 data. J.W. wrote the manuscript. S.H., J.T., and Y.H. revised the manuscript. All
454 authors have read and approved the final manuscript.

455 **Acknowledgments**

456 This research was supported by the National Natural Science Foundation of
457 China (31860032 and 32360045).

458 **Conflict of interest**

459 The authors declare no conflict of interest.

460 **Data availability statement**

461 All relevant data can be found within the manuscript and its supporting materials.

462

463

464

465

466 **References**

467 Boller T and He SY (2009) Innate immunity in plants: an arms race between
468 pattern recognition receptors in plants and effectors in microbial pathogens.
469 Science **324**:742-744.

470 Cernadas RA, Doyle EL, Nino-Liu DO, Wilkins KE, Bancroft T, Wang L, Schmidt
471 CL, Caldo R, Yang B, White FF, Nettleton D, Wise RP and Bogdanove AJ (2014)
472 Code-assisted discovery of tal effector targets in bacterial leaf streak of rice
473 reveals contrast with bacterial blight and a novel susceptibility gene. PLoS
474 Pathog **10**:e1003972.

475 Chen JG, Ullah H, Temple B, Liang J, Guo J, Alonso JM, Ecker JR and Jones
476 AM (2006) RACK1 mediates multiple hormone responsiveness and
477 developmental processes in *Arabidopsis*. J Exp Bot **57**:2697-2708.

478 Cheng Z, Li JF, Niu Y, Zhang XC, Woody OZ, Xiong Y, Djonovic S, Millet Y, Bush
479 J, McConkey BJ, Sheen J and Ausubel FM (2015) Pathogen-secreted
480 proteases activate a novel plant immune pathway. Nature **521**:213-216.

481 Cui Y, Zou L, Zou H, Li Y, Zakria M and Chen G (2013) HrpE3 is a type III
482 effector protein required for full virulence of *Xanthomonas oryzae* pv. *oryzicola*
483 in rice. Mol Plant Pathol **14**:678-692.

484 Deb S, Ghosh P, Patel HK and Sonti RV (2020) Interaction of theXanthomonas
485 effectors XopQ and XopX results in induction of rice immune responses. Plant
486 J **104**:332-350.

487 Dodds PN and Rathjen JP (2010) Plant immunity: towards an integrated view
488 of plant-pathogen interactions. Nat Rev Genet **11**:539-548.

489 Fu M, Tian Y, Wu D, Xue F, Gao H and Liang W (2025) The RNA-binding protein
490 OsDMCK1 is required for meiotic cytokinesis by regulating cell plate formation
491 in rice. Plant J **123**:e70448.

492 Fu Y, Zhu W, Zhou Y, Su Y, Li Z, Zhang D, Zhang D, Shen J and Liang J (2024)
493 RACK1A promotes hypocotyl elongation by scaffolding light signaling
494 components in *Arabidopsis*. J Integr Plant Biol **66**:956-972.

495 Gao M, He Y, Yin X, Zhong X, Yan B, Wu Y, Chen J, Li X, Zhai K, Huang Y,

496 Gong X, Chang H, Xie S, Liu J, Yue J, Xu J, Zhang G, Deng Y, Wang E,
497 Tharreau D, Wang G, Yang W and He Z (2021) Ca2+ sensor-mediated ROS
498 scavenging suppresses rice immunity and is exploited by a fungal effector. Cell
499 **184**:5391-5404.

500 Guo R and Sun W (2017) Sumoylation stabilizes RACK1B and enhance its
501 interaction with RAP2.6 in the abscisic acid response. Sci Rep **7**:44090.

502 He Z, Zhang Z, Vale G, San SB, Chen X and Pasupuleti J (2023) Editorial:
503 Disease and pest resistance in rice. Front Plant Sci **14**:1333904.

504 Islas-Flores T, Rahman A, Ullah H and Villanueva MA (2015) The receptor for
505 activated c kinase in plant signaling: TALE of a promiscuous little molecule.
506 Front Plant Sci **6**:1090.

507 Jones JD and Dangl JL (2006) The plant immune system. Nature **444**:323-329.

508 Kay S and Bonas U (2009) How *Xanthomonas* type III effectors manipulate the
509 host plant. Curr Opin Microbiol **12**:37-43.

510 Kim JG, Li X, Roden JA, Taylor KW, Aakre CD, Su B, Lalonde S, Kirik A, Chen
511 Y, Baranage G, McLane H, Martin GB and Mudgett MB (2009) *Xanthomonas*
512 T3S Effector XopN Suppresses PAMP-Triggered Immunity and Interacts with a
513 Tomato Atypical Receptor-Like Kinase and TFT1. Plant Cell **21**:1305-1323.

514 Leong JX, Raffeiner M, Spinti D, Langin G, Franz-Wachtel M, Guzman AR, Kim
515 JG, Pandey P, Minina AE, Macek B, Hafren A, Bozkurt TO, Mudgett MB, Bornke
516 F, Hofius D and Ustun S (2022) A bacterial effector counteracts host autophagy
517 by promoting degradation of an autophagy component. EMBO J **41**:e110352.

518 Li B, Meng X, Shan L and He P (2016) Transcriptional Regulation of Pattern-
519 Triggered Immunity in Plants. Cell Host Microbe **19**:641-650.

520 Li GB, He JX, Wu JL, Wang H, Zhang X, Liu J, Hu XH, Zhu Y, Shen S, Bai YF,
521 Yao ZL, Liu XX, Zhao JH, Li DQ, Li Y, Huang F, Huang YY, Zhao ZX, Zhang JW,

522 Zhou SX, Ji YP, Pu M, Qin P, Li S, Chen X, Wang J, He M, Li W, Wu XJ, Xu ZJ,
523 Wang WM and Fan J (2022) Enhanced production of OsRACK1A, an effector-
524 targeted scaffold protein that promotes OsRBOHB-mediated ROS production,
525 confers rice floral resistance to false smut disease without yield penalty. Mol
526 Plant **15**:1790-1806.

527 Li N, Lin Z, Yu P, Zeng Y, Du S and Huang L (2023) The multifarious role of
528 callose and callose synthase in plant development and environment
529 interactions. Front Plant Sci **14**:1183402.

530 Li S, Wang Y, Wang S, Fang A, Wang J, Liu L, Zhang K, Mao Y and Sun W
531 (2015) The type III effector AvrBs2 in *Xanthomonas oryzae* pv. *oryzicola*
532 suppresses rice immunity and promotes disease development. Mol Plant
533 Microbe In **28**:869-880.

534 Liao Z, Li J, Mo X, Ni Z, Jiang W, He Y and Huang S (2020) Type III effectors
535 xopN and avrBS2 contribute to the virulence of *Xanthomonas oryzae* pv.
536 *oryzicola* strain GX01. Res Microbiol **171**:102-106.

537 Liu H, Lu C, Li Y, Wu T, Zhang B, Liu B, Feng W, Xu Q, Dong H, He S, Chu Z
538 and Ding X (2022) The bacterial effector AvrRxo1 inhibits vitamin B6
539 biosynthesis to promote infection in rice. Plant Commun **3**:100324.

540 Liu L, Li Y, Xu Z, Chen H, Zhang J, Manion B, Liu F, Zou L, Fu ZQ and Chen G
541 (2022) The *Xanthomonas* type III effector XopAP prevents stomatal closure by
542 interfering with vacuolar acidification. J Integr Plant Biol **64**:1994-2008.

543 Liu W, Liu J, Triplett L, Leach JE and Wang GL (2014) Novel insights into rice
544 innate immunity against bacterial and fungal pathogens. Annu Rev Phytopathol
545 **52**:213-241.

546 Lo Presti L, Lanver D, Schweizer G, Tanaka S, Liang L, Tollot M, Zuccaro A,
547 Reissmann S and Kahmann R (2015) Fungal effectors and plant susceptibility.
548 Annu Rev Plant Biol **66**:513-545.

549 Ma Z, Qin G, Zhang Y, Liu C, Wei M, Cen Z, Yan Y, Luo T, Li Z, Liang H, Huang
550 D and Deng G (2021) Bacterial leaf streak 1 encoding a mitogen-activated
551 protein kinase confers resistance to bacterial leaf streak in rice. Plant J
552 **107**:1084-1101.

553 Nakashima A, Chen L, Thao NP, Fujiwara M, Wong HL, Kuwano M, Umemura
554 K, Shirasu K, Kawasaki T and Shimamoto K (2008) RACK1 functions in rice
555 innate immunity by interacting with the Rac1 immune complex. Plant Cell
556 **20**:2265-2279.

557 Oliva R, Ji C, Atienza-Grande G, Huguet-Tapia JC, Perez-Quintero A, Li T, Eom
558 JS, Li C, Nguyen H, Liu B, Auguy F, Sciallano C, Luu VT, Dossa GS, Cunnac S,
559 Schmidt SM, Slamet-Loedin IH, Vera CC, Szurek B, Frommer WB, White FF
560 and Yang B (2019) Broad-spectrum resistance to bacterial blight in rice using
561 genome editing. Nat Biotechnol **37**:1344-1350.

562 Robert X and Gouet P (2014) Deciphering key features in protein structures
563 with the new ENDscript server. Nucleic Acids Res **42**:W320-W324.

564 Spoel SH and Dong X (2012) How do plants achieve immunity? Defence
565 without specialized immune cells. Nat Rev Immunol **12**:89-100.

566 Sun H, Zhu X, Li C, Ma Z, Han X, Luo Y, Yang L, Yu J and Miao Y (2021)
567 *Xanthomonas* effector XopR hijacks host actin cytoskeleton via complex
568 coacervation. Nat Commun **12**:4064.

569 Taylor KW, Kim J, Su XB, Aakre CD, Roden JA, Adams CM and Mudgett MB
570 (2012) Tomato TFT1 is required for PAMP-triggered immunity and mutations
571 that prevent T3S effector XopN from binding to TFT1 attenuate *Xanthomonas*
572 virulence. PLoS Pathog **8**:e1002768.

573 Triplett LR, Cohen SP, Heffelfinger C, Schmidt CL, Huerta AI, Tekete C, Verdier
574 V, Bogdanove AJ and Leach JE (2016) A resistance locus in the American
575 heirloom rice variety Carolina Gold Select is triggered by TAL effectors with

576 diverse predicted targets and is effective against African strains of
577 *Xanthomonas oryzae* pv. *oryzicola*. Plant J **87**:472-483.

578 Tsuda K and Katagiri F (2010) Comparing signaling mechanisms engaged in
579 pattern-triggered and effector-triggered immunity. Curr Opin Plant Biol **13**:459-
580 465.

581 Wamaitha MJ, Yamamoto R, Wong HL, Kawasaki T, Kawano Y and Shimamoto
582 K (2012) OsRap2.6 transcription factor contributes to rice innate immunity
583 through its interaction with Receptor for Activated Kinase-C 1 (RACK1). Rice
584 **5**:35.

585 Wang J, Liao Z, Jin X, Liao L, Zhang Y, Zhang R, Zhao X, Qin H, Chen J, He Y,
586 Zhuang C, Tang J and Huang S (2024) *Xanthomonas oryzae* pv. *oryzicola*
587 effector Tal10a directly activates rice OsHXK5 expression to facilitate
588 pathogenesis. Plant J **119**:2423-2436.

589 Wang S, Li S, Wang J, Li Q, Xin XF, Zhou S, Wang Y, Li D, Xu J, Luo ZQ, He
590 SY and Sun W (2021) A bacterial kinase phosphorylates OSK1 to suppress
591 stomatal immunity in rice. Nat Commun **12**:5479.

592 Wang W, Feng B, Zhou JM and Tang D (2020) Plant immune signaling:
593 Advancing on two frontiers. J Integr Plant Biol **62**:2-24.

594 Wang Y, Pruitt RN, Nurnberger T and Wang Y (2022) Evasion of plant immunity
595 by microbial pathogens. Nat Rev Microbiol **20**:449-464.

596 Xie H, Lin C, Lu W, Han Z, Wei D, Huo X, Li T, Zhang J, He Y and Chen C (2023)
597 OsBLS6.2: A rice bacterial leaf streak resistance gene identified by GWAS and
598 RNA-seq. Crop Journal **11**:1862-1871.

599 Xie X, Chen Z, Cao J, Guan H, Lin D, Li C, Lan T, Duan Y, Mao D and Wu W
600 (2014) Toward the positional cloning of qBlsr5a, a QTL underlying resistance to
601 bacterial leaf streak, using overlapping sub-CSSLs in rice. PLoS One **9**:e95751.

602 Xie X, Ma X, Zhu Q, Zeng D, Li G and Liu YG (2017) CRISPR-GE: A Convenient
603 Software Toolkit for CRISPR-Based Genome Editing. Mol Plant **10**:1246-1249.

604 Yoshihisa A, Yoshimura S, Shimizu M, Sato S, Matsuno S, Mine A, Yamaguchi
605 K and Kawasaki T (2022) The rice OsERF101 transcription factor regulates the
606 NLR Xa1-mediated immunity induced by perception of TAL effectors. New
607 Phytol **236**:1441-1454.

608 Yuan S, Linquist BA, Wilson LT, Cassman KG, Stuart AM, Pede V, Miro B, Saito
609 K, Agustiani N, Aristya VE, Krisnadi LY, Zanon AJ, Heinemann AB, Carracelas
610 G, Subash N, Brahmanand PS, Li T, Peng S and Grassini P (2021) Sustainable
611 intensification for a larger global rice bowl. Nat Commun **12**:7163.

612 Zhang H, Sun B, Wu W, Li Y, Yin Z, Lu C, Zhao H, Kong L and Ding X (2024)
613 The MYB transcription factor OsMYBxoc1 regulates resistance to *Xoc* by
614 directly repressing transcription of the iron transport gene OsNRAMP5 in rice.
615 Plant Commun **5**:100859.

616

617 **Figure legends**

618 **Figure 1. XopN suppresses immune responses in rice. (a)** Callose
619 deposition in rice leaves at 72 hours post-inoculation with the *Xoc* wild-type
620 strain GX01, the Δ*xopN* mutant, and the complemented strain CΔ*xopN*. Scale
621 bar, 100 μm. **(b)** Quantification of callose deposits per leaf. Data represent
622 means ± standard deviations, n=5. Asterisks denote statistically significant
623 differences between the Δ*xopN* mutant and either the wild-type or
624 complemented strain (**, $P < 0.01$, Student's *t*-test). **(c)** DAB staining of rice
625 leaves at 72 hours post-inoculation with GX01, Δ*xopN*, and CΔ*xopN*. **(d, e)**
626 Relative expression levels of *OsPBZ1* and *OsPAL1* in NIP rice at 24 hours post-
627 inoculation with GX01, Δ*xopN*, and CΔ*xopN*. Rice actin was used as an internal
628 control. Data represent means ± standard deviations, n = 3. Asterisks indicate

629 significant differences compared to wild-type or complemented strains (**, $P <$
630 0.01, Student's *t*-test). **(f)** Subcellular localization of XopN in planta. Rice
631 protoplasts were transfected with a construct expressing XopN fused to the N-
632 terminus of GFP (XopN-GFP). At 24 h post-transfection, fluorescence was
633 visualized by confocal laser scanning microscopy. Scale bars, 10 μm.

634 **Figure 2. XopN physically interacts with OsRACK1B. (a)** Y2H analysis
635 showing the interaction between XopN and OsRACK1B. Yeast strain Y2HGold
636 was co-transformed with the indicated plasmid combinations and cultured on
637 SD/-Leu-Trp and the selective medium SD/-Leu-Trp-His-Ade. Plates were
638 incubated at 30 °C for 3 days prior to imaging. The p53/T combination served
639 as a positive control, and Lam/T as a negative control. EV, empty vector control.
640 SD/-LW, SD/-Leu-Trp; SD/-LWHA, SD/-Leu-Trp-His-Ade. **(b)** BiFC assay
641 demonstrating the in vivo interaction of XopN with OsRACK1B in rice
642 protoplasts. XopN was fused to the N-terminal fragment of YFP (nYFP), and
643 OsRACK1B to the C-terminal fragment (cYFP). Reconstituted YFP
644 fluorescence was visualized by confocal microscopy 20 hours post-
645 transformation. Scale bar, 10 μm. EV, empty vector control. **(c)** In vitro pull-
646 down assay confirming the physical interaction between XopN and OsRACK1B.
647 Recombinant His-tagged XopN and GST-tagged OsRACK1B, expressed and
648 purified from *E. coli*, were subjected to pull-down using Ni-NTA resin. Bound
649 proteins were detected by immunoblotting with anti-GST and anti-His
650 antibodies. **(d)** Y2H assay showing the interaction between OsRACK1B and
651 truncated fragments of XopN. **(e)** Y2H assay demonstrating the interaction
652 between XopN and truncated variants of OsRACK1B. Yeast strain Y2HGold
653 was co-transformed with the indicated plasmid combinations and cultured on
654 SD/-Leu-Trp and the selective medium SD/-Leu-Trp-His-Ade. Plates were
655 incubated at 30 °C for 3 days prior to imaging. SD/-LW, SD/-Leu-Trp; SD/-LWHA,
656 SD/-Leu-Trp-His-Ade.

657 **Figure 3. Overexpression of *OsRACK1B* enhances rice resistance to *Xoc*.**

658 **(a, b)** Expression dynamics of *OsRACK1B* in rice leaves following inoculation
659 with the wild-type *Xoc* strain GX01 or the T3SS-deficient mutant strain Δ*hrcC*.
660 Rice actin was used as an internal control. Data represent means ± standard
661 deviations, n = 3. Asterisks indicate statistically significant differences (**, $P <$
662 0.01, Student's *t*-test). **(c)** Subcellular localization of OsRACK1B in planta. Rice
663 protoplasts were transfected with a construct expressing OsRACK1B fused to
664 the N-terminus of CFP (OsRACK1B-CFP) and co-expressed with the nuclear
665 marker ABF1-mCherry. Fluorescence was detected by confocal laser scanning
666 microscopy at 24 h post-transfection. Scale bars, 10 μm. **(d)** Relative
667 expression of *OsRACK1B* in wild-type NIP and transgenic overexpression lines.
668 Rice actin was used as an internal control. Data represent means ± standard
669 deviations, n = 3. Asterisks indicate statistically significant differences (**, $P <$
670 0.01, Student's *t*-test). **(e)** Phenotypes of lesion expansion in the NIP and
671 *OsRACK1B* overexpression lines at 14 days post-inoculation with GX01. **(f)**
672 Lesion lengths in the NIP and *OsRACK1B* overexpression lines at 14 days post-
673 inoculation with GX01. Data are displayed as boxplots with individual data
674 points. Error bars represent maximum and minimum values. Center line,
675 median; box limits, 25th and 75th percentiles. Asterisk indicate a significant
676 difference between the NIP and *OsRACK1B* overexpression lines (**, $P < 0.01$,
677 Student's *t*-test, n = 20).

678 **Figure 4. Loss of *OsRACK1B* function compromises rice resistance to**
679 ***Xoc*. (a)** Generation of *OsRACK1B* homozygous knockout mutants via
680 CRISPR-Cas9 editing. The schematic illustrates the *OsRACK1B* gene structure
681 and the targeted genomic locus. Blue nucleotides denote the protospacer
682 adjacent motif (PAM); red letters indicate inserted bases; hyphens represent
683 nucleotide deletions. **(b)** Phenotypes of lesion expansion in the NIP and
684 *OsRACK1B* edited mutants at 14 days post-inoculation with GX01. **(c)** Lesion
685 lengths in the NIP and *OsRACK1B* edited mutants at 14 days post-inoculation
686 with GX01. Data are displayed as boxplots. Error bars represent maximum and

687 minimum values. Center line, median; box limits, 25th and 75th percentiles.
688 Asterisks indicate a significant difference between the NIP and OsRACK1B
689 edited mutants (**, $P < 0.01$, Student's *t*-test, n = 20).

690 **Figure 5. *OsRACK1B* is required for rice immune responses to *Xoc.* (a)**
691 Callose deposition in wild-type NIP and *OsRACK1B* knockout lines at 48 hours
692 post-inoculation with Δ*hrcC*. Scale bar, 50 μm. **(b)** Quantification of callose
693 deposits per leaf in NIP and OsRACK1B knockout plants. Data represent
694 means ± standard deviations, n=5. Asterisks denote statistically significant
695 differences between NIP and *OsRACK1B* knockout lines (**, $P < 0.01$,
696 Student's *t*-test). **(c)** DAB staining showing hydrogen peroxide (H_2O_2)
697 accumulation in NIP and *OsRACK1B* knockout lines at 48 hours post-
698 inoculation with Δ*hrcC*. **(d, e)** Relative transcript levels of *OsPBZ1* and *OsPAL1*
699 in NIP and *OsRACK1B* knockout lines at 24 hours post-inoculation with Δ*hrcC*.
700 Rice *actin* was used as an internal control. Data represent means ± standard
701 deviations, n=3. Asterisks denote statistically significant differences between
702 NIP and *OsRACK1B* knockout lines (**, $P < 0.01$, Student's *t*-test).

703 **Figure 6. XopN competes with OsRap2.6 for binding to OsRACK1B. (a)**
704 AlphaFold predicts the effect of XopN on the OsRACK1B–Rap2.6 interaction.
705 **(b)** Y3H assay was performed to evaluate the competitive binding dynamics
706 between XopN and OsRap2.6 for OsRACK1B. Yeast strain Y2HGold was co-
707 transformed with the indicated plasmid combinations and cultured on SD/-Leu-
708 Trp-Met and the selective medium SD/-Leu-Trp-His-Ade-Met. Plates were
709 incubated at 30 °C for 3 days prior to imaging. EV, empty vector control. SD/-
710 LWM, SD/-Leu-Trp-Met; SD/-LWHAM, SD/-Leu-Trp-His-Ade-Met. **(c)**
711 Schematic summary of XopN function in rice–*Xoc* interactions. During infection,
712 the type III effector XopN is secreted by *Xoc* and translocated into rice cells,
713 where it targets the scaffold protein OsRACK1B, a key component of rice
714 immune signaling against *Xoc*. XopN binds to OsRACK1B in a manner that
715 competitively interferes with the recruitment of the transcription factor

716 OsRap2.6, thereby disrupting the formation of an OsRACK1B–OsRap2.6
717 immune complex. This disruption attenuates downstream immune responses,
718 including callose deposition, ROS accumulation, and the transcriptional
719 activation of defense-related genes, ultimately facilitating bacterial colonization
720 of host tissue.

721 **Supporting Information**

722 Additional Supporting Information may be found online in the Supporting
723 Information section at the end of the article.

724 **Figure S1.** Sequence alignment of XopN and its homologs.

725 **Figure S2.** Sequence analysis of OsRACK1B.

726 **Figure S3.** Validation of the interaction between OsRACK1B and OsRap2.6.

727 **Table S1** Primers used in this study.

728

729

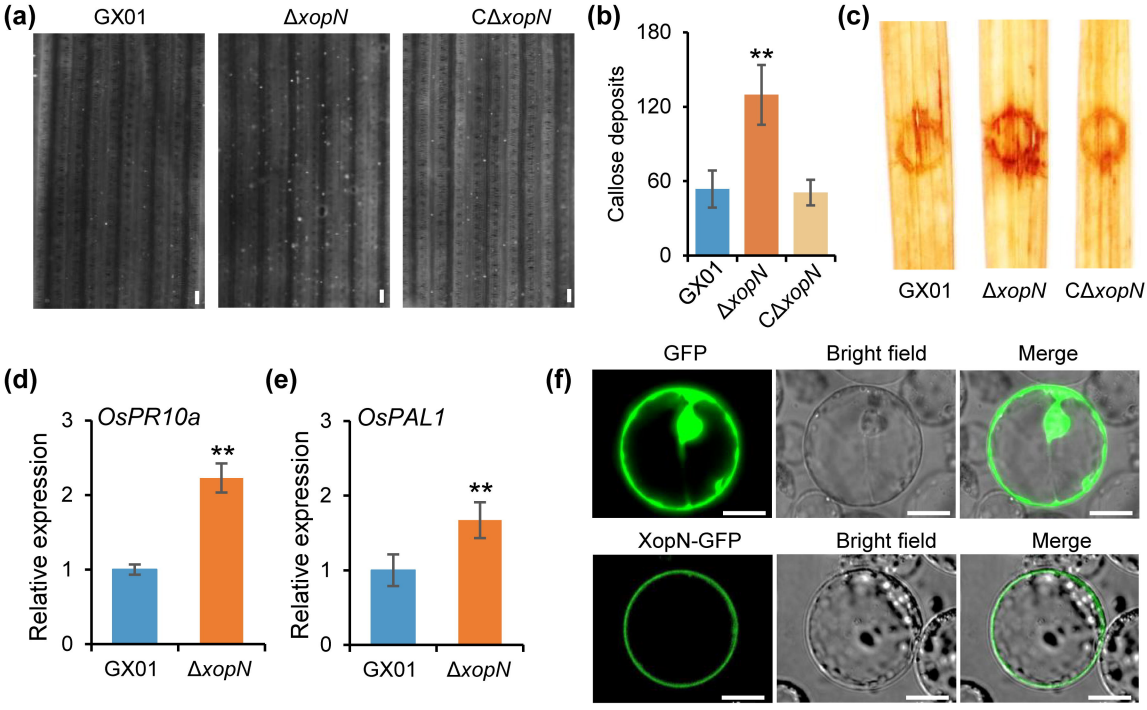
(a)
GX01
ΔxopN
CΔxopN
(b)
Callose deposits
180
120
60
0
**
GX01
ΔxopN
CΔxopN
(c)
GX01
ΔxopN
CΔxopN
(d)
OsPR10a
Relative expression
3
2
1
0
**
GX01
ΔxopN
(e)
OsPAL1
Relative expression
3
2
1
0
**
GX01
ΔxopN
(f)
GFP
Bright field
Merge
XopN-GFP
Bright field
Merge

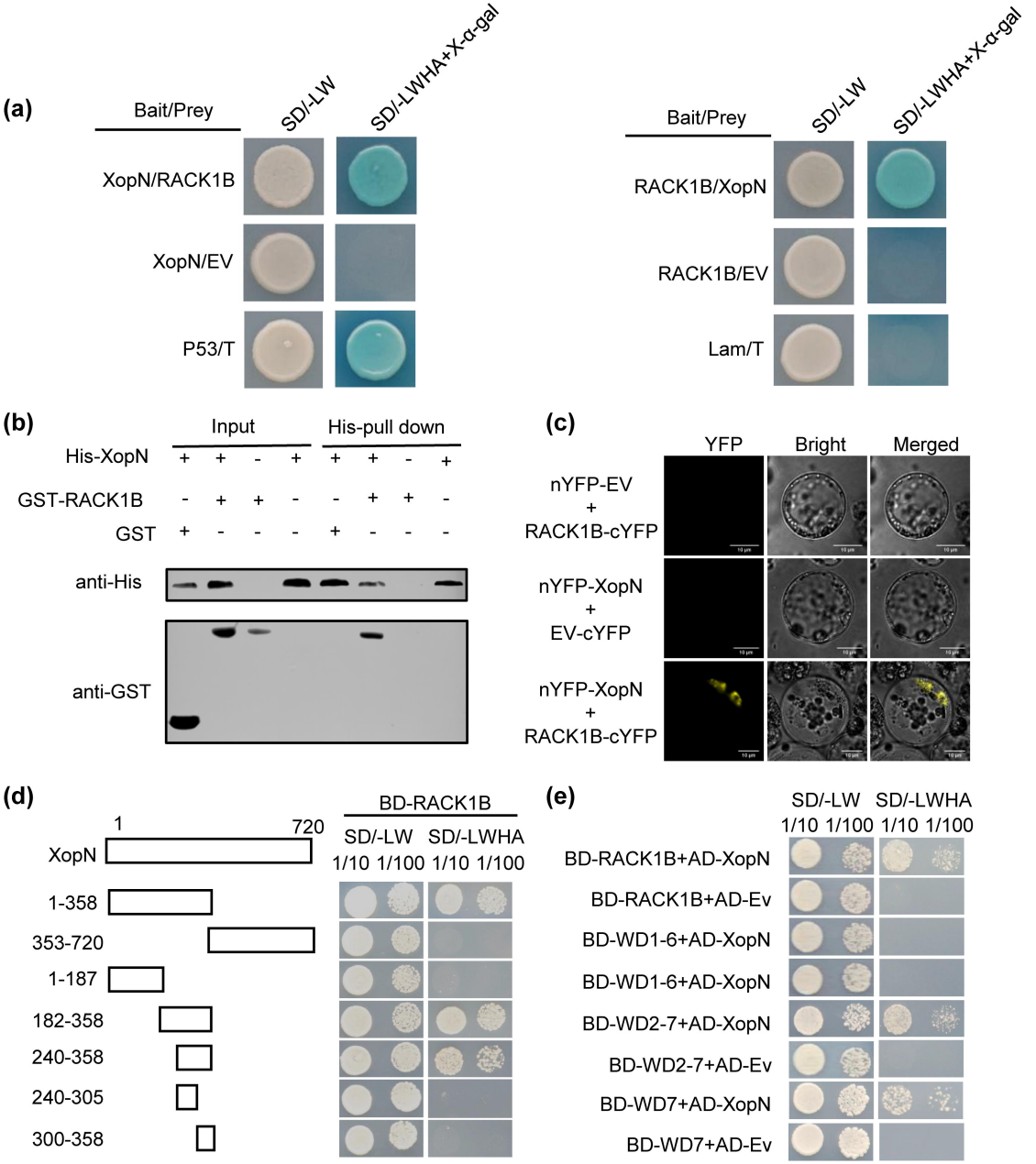
(a)
Bait/Prey
SD/-LW
SD/-LWHA+X-α-gal
XopN/RACK1B
XopN/EV
P53/T
Bait/Prey
SD/-LW
SD/-LWHA+X-α-gal
RACK1B/XopN
RACK1B/EV
Lam/T
(b)
Input
His-pull down
His-XopN + + - + + + - +
GST-RACK1B - + + - - + + -
GST + - - - + - - -
anti-His
anti-GST
(c)
YFP
Bright
Merged
nYFP-EV + RACK1B-cYFP
nYFP-XopN + EV-cYFP
nYFP-XopN + RACK1B-cYFP
(d)
BD-RACK1B
1
720
XopN
SD/-LW
SD/-LWHA
1/10 1/100 1/10 1/100
1-358
353-720
1-187
182-358
240-358
240-305
300-358
(e)
SD/-LW
SD/-LWHA
1/10 1/100 1/10 1/100
BD-RACK1B+AD-XopN
BD-RACK1B+AD-Ev
BD-WD1-6+AD-XopN
BD-WD1-6+AD-XopN
BD-WD2-7+AD-XopN
BD-WD2-7+AD-Ev
BD-WD7+AD-XopN
BD-WD7+AD-Ev

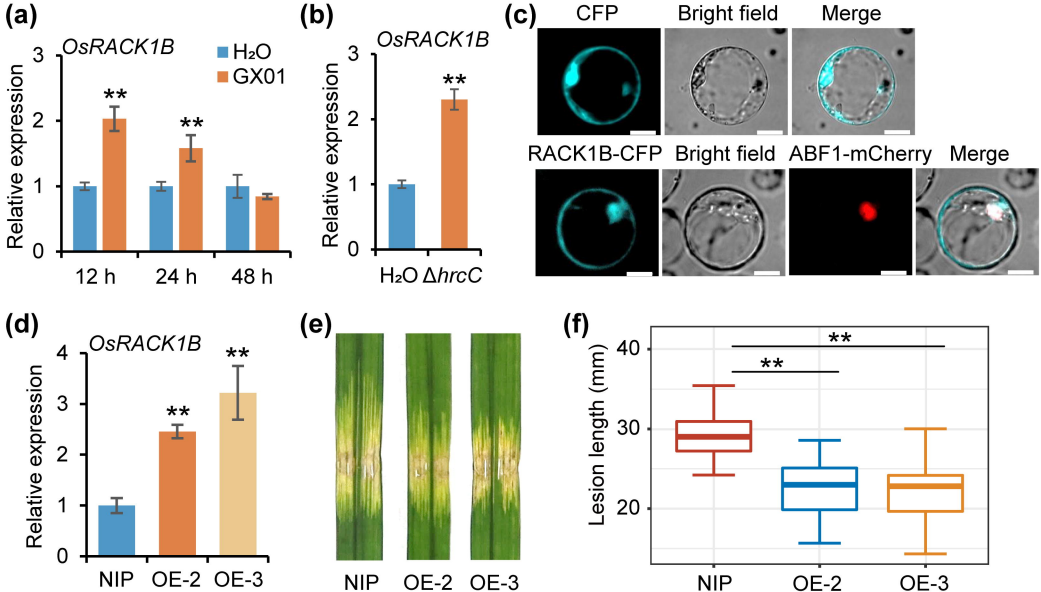
(a)
OsRACK1B
H₂O
GX01
Relative expression
0
1
2
3
**
**
12 h
24 h
48 h
(b)
OsRACK1B
Relative expression
0
1
2
3
**
H₂O
ΔhrcC
(c)
CFP
Bright field
Merge
RACK1B-CFP
Bright field
ABF1-mCherry
Merge
(d)
OsRACK1B
Relative expression
0
1
2
3
4
**
**
NIP
OE-2
OE-3
(e)
NIP
OE-2
OE-3
(f)
Lesion length (mm)
20
30
40
**
**
NIP
OE-2
OE-3

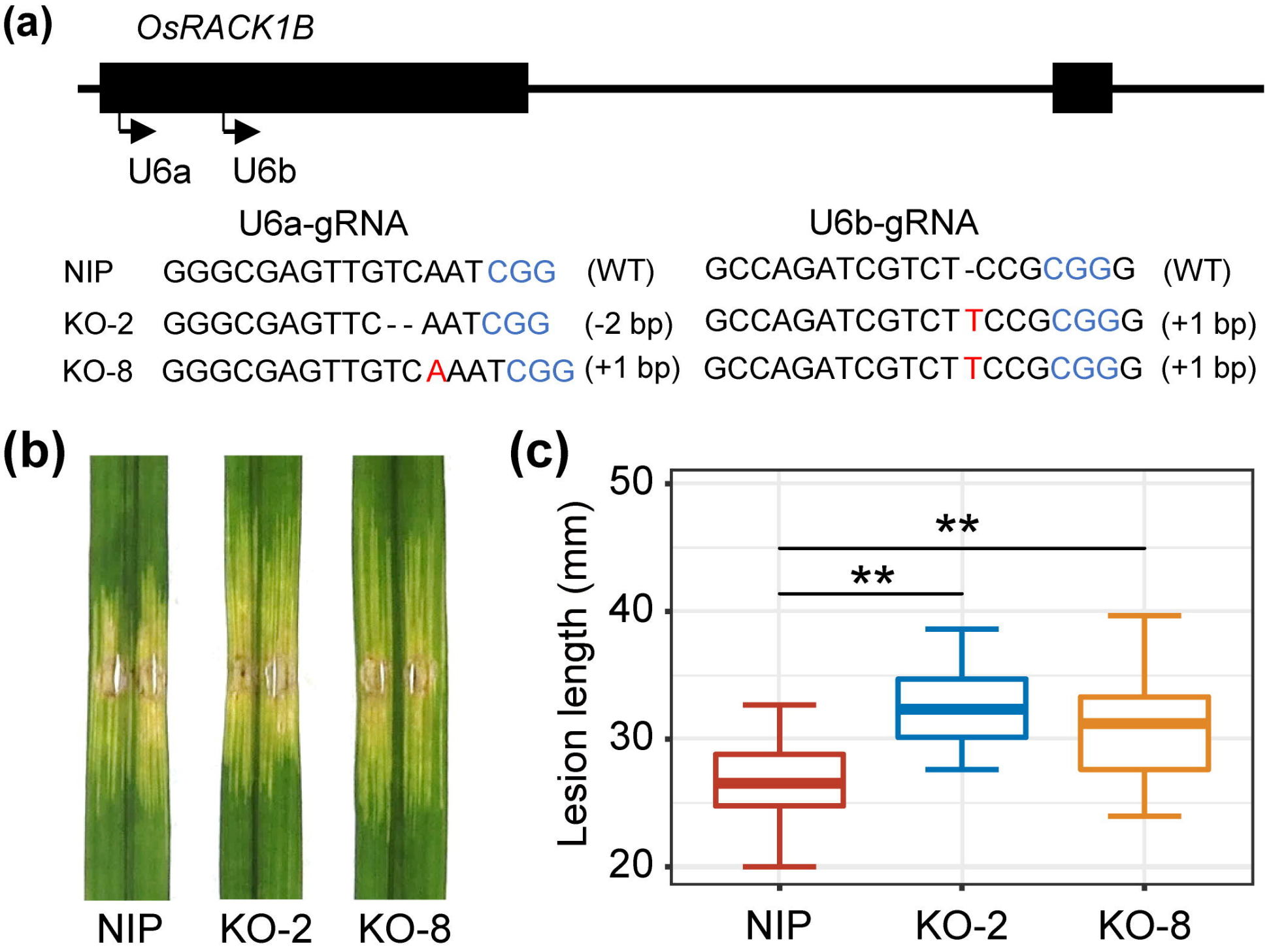
(a)
OsRACK1B
U6a
U6b
U6a-gRNA
U6b-gRNA
NIP GGGCGAGTTGTCAATCGG (WT) GCCAGATCGTCT-CCGCGGG (WT)
KO-2 GGGCGAGTTC--AATCGG (-2 bp) GCCAGATCGTCTTCCGCGGG (+1 bp)
KO-8 GGGCGAGTTGTCAAATCGG (+1 bp) GCCAGATCGTCTTCCGCGGG (+1 bp)
(b)
NIP
KO-2
KO-8
(c)
Lesion length (mm)
50
40
30
20
**
**
NIP
KO-2
KO-8

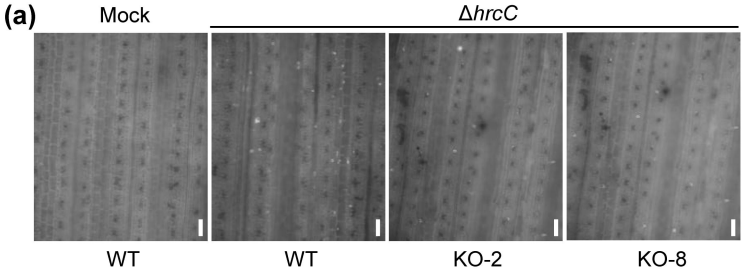
(a)
Mock
ΔhrcC
WT
WT
KO-2
KO-8

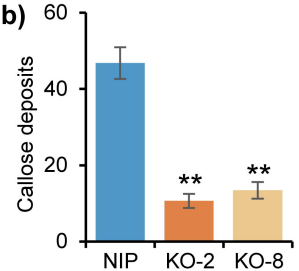
(b)
Callose deposits
60
40
20
0
**
**
NIP
KO-2
KO-8

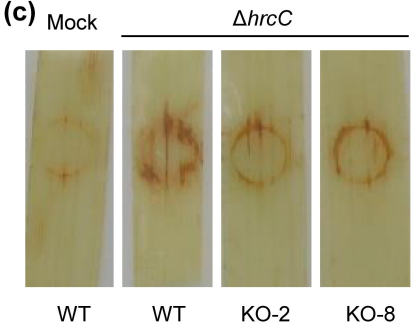
(c)
Mock
ΔhrcC
WT
WT
KO-2
KO-8

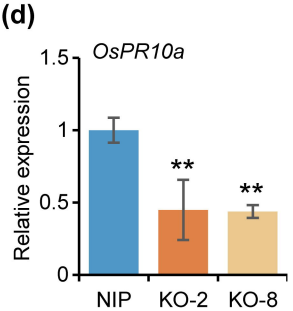
(d)
OsPR10a
Relative expression
1.5
1
0.5
0
**
**
NIP
KO-2
KO-8

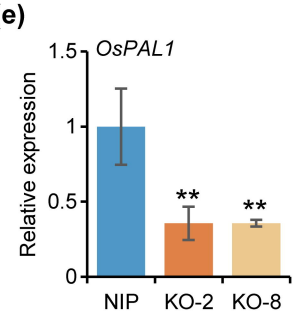
(e)
OsPAL1
Relative expression
1.5
1
0.5
0
**
**
NIP
KO-2
KO-8

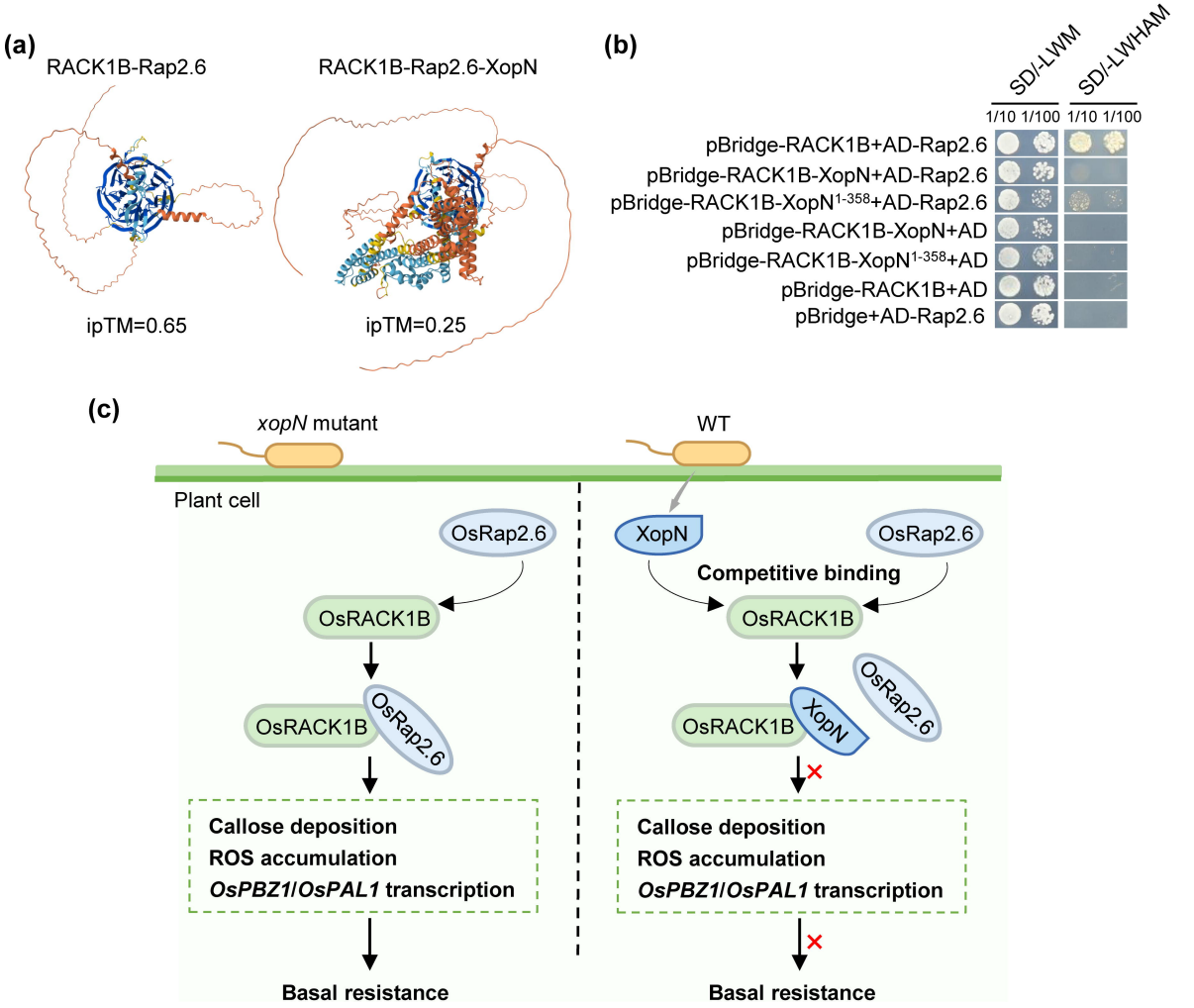
(a)
RACK1B-Rap2.6
RACK1B-Rap2.6-XopN
ipTM=0.65
ipTM=0.25
(b)
SD/-LWM
SD/-LWHAM
1/10 1/100 1/10 1/100
pBridge-RACK1B+AD-Rap2.6
pBridge-RACK1B-XopN+AD-Rap2.6
pBridge-RACK1B-XopN1-358+AD-Rap2.6
pBridge-RACK1B-XopN+AD
pBridge-RACK1B-XopN1-358+AD
pBridge-RACK1B+AD
pBridge+AD-Rap2.6
(c)
xopN mutant
WT
Plant cell
OsRap2.6
OsRACK1B
OsRACK1B
OsRap2.6
Callose deposition
ROS accumulation
OsPBZ1/OsPAL1 transcription
Basal resistance
XopN
OsRap2.6
Competitive binding
OsRACK1B
OsRACK1B
XopN
OsRap2.6
Callose deposition
ROS accumulation
OsPBZ1/OsPAL1 transcription
Basal resistance